

# Push it to the Demonstrated Limit: Multimodal Visuotactile Imitation Learning with Force Matching

Trevor Ablett<sup>1,2</sup>, Oliver Limoyo<sup>1,2</sup>, Adam Sigal<sup>1</sup>, Affan Jilani<sup>3</sup>,  
Jonathan Kelly<sup>2</sup>, Kaleem Siddiqi<sup>1,3</sup>, Francois Hogan<sup>1</sup>, Gregory Dudek<sup>1,3</sup>

**Abstract**—Optical tactile sensors have emerged as an effective means to acquire dense contact information during robotic manipulation. A recently-introduced ‘see-through-your-skin’ (STS) variant of this type of sensor has both visual and tactile modes, enabled by leveraging a semi-transparent surface and controllable lighting. In this work, we investigate the benefits of pairing visuotactile sensing with imitation learning for contact-rich manipulation tasks. First, we use tactile force measurements and a novel algorithm during kinesthetic teaching to yield a force profile that better matches that of the human demonstrator. Second, we add visual/tactile STS mode switching as a control policy output, simplifying the application of the sensor. Finally, we study multiple observation configurations to compare and contrast the value of visual/tactile data (both with and without mode switching) with visual data from a wrist-mounted eye-in-hand camera. We perform an extensive series of experiments on a real robotic manipulator with door-opening and closing tasks, including over 3,000 real test episodes. Our results highlight the importance of tactile sensing for imitation learning, both for data collection to allow force matching, and for policy execution to allow accurate task feedback.

## I. INTRODUCTION

When humans interact with articulated objects such as doors or drawers, their hands and fingers commonly slip, roll, and generate significant shear and normal forces relative to the handle. To achieve similar behaviour, robotic manipulators should integrate high-resolution tactile feedback as well as corresponding motor policies to quickly act in response to this feedback. Optical tactile sensors [1] combine a gel-based material with a small, inexpensive camera to yield rich tactile information [2] and are able to provide the requisite feedback for dexterous manipulation [3], [4]. A recently-introduced see-through-your-skin (STS) optical sensor variant combines visual sensing with tactile sensing by leveraging a transparent membrane and controllable lighting. This sensor enables perception of the full interaction, from approach, through initial contact, to grasping.

In this paper, we investigate how to leverage visuotactile sensing for imitation learning (IL) on a real robotic platform for contact-rich manipulation tasks. We focus on opening and closing cabinet doors with a single robotic finger, both of which involve complex frictional dynamics where the

<sup>1</sup>Authors are with Samsung AI Centre, Montreal, QC M3H 5T6, Canada. Email: {t.ablett,o.limoyo}@partner.samsung.com, {adam.sigal,f.hogan,greg.dudek}@samsung.com

<sup>2</sup>Authors are with the Robotics Institute (RI) at the University of Toronto, Toronto, ON M5S 1A4, Canada. Email: first-name.last-name@robotics.utiias.utoronto.ca

<sup>3</sup>Authors are with McGill University, Montreal, QC H3A 089, Canada. Email: first-name.last-name@mail.mcgill.ca

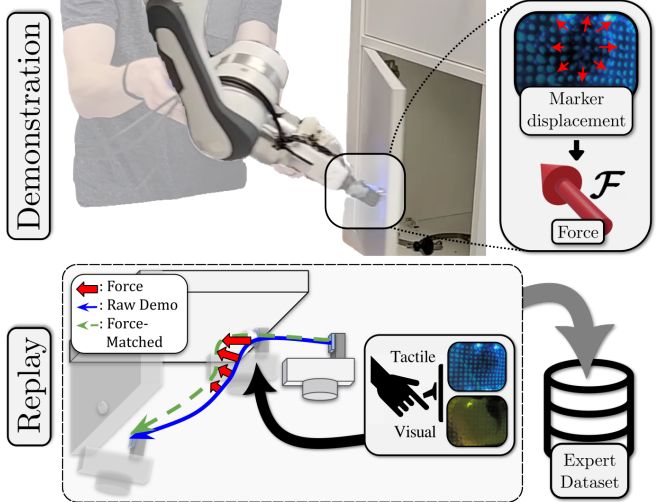


Fig. 1: Our system: (i) demonstrations are collected through kinesthetic teaching, with a signal proportional to force read by the see-through-your-skin sensor (STS) in tactile mode, and (ii) demonstrations are replayed with force matching enabled, while the expert simultaneously provides a mode-switch label. These replayed, force-matched trajectories form an expert dataset for imitation learning with both visual and tactile data.

robot needs to reason about interaction forces. Human-based expert demonstrations for IL can be collected in a variety of ways, though most methods fall generally into the kinesthetic teaching or teleoperation categories [5].

Because kinesthetic teaching provides haptic environmental feedback to the demonstrator, it can allow for higher-quality demonstrations than teleoperation, which requires a proxy for true haptic feedback [6], [7]. Unfortunately, kinesthetic teaching methods typically only measure a demonstrator’s motion, without considering the *force* placed on the environment by the robot. To match the demonstrator’s force profile, we require a means of measuring robot to environment forces, in addition to a mechanism for reproducing those forces. Our first contribution is a *force matching* algorithm that modifies the recorded poses from kinesthetic teaching, creating new *desired* poses that are programmed to recover the recorded forces when used as input to a Cartesian impedance controller. We measure a signal which is proportional to force (based on surface depth, see Section III-D for details), using an STS sensor in tactile mode, because: (i) standard methods for measuring force-torque will be corrupted by the human’s own forces (see Fig. 3), (ii) an STS is an order of magnitude less expensive than a similarly-mounted force-torque sensor, and (iii) the



Fig. 2: Our STS sensor before and during contact with a cabinet knob during a door opening task. In visual mode, the camera sees through the gel and allows (1) finding and (2) reaching the knob, while tactile mode provides feedback, via gel deformation and dot displacement, upon (3) initial contact and (4) during door opening.

STS can be separately used for policy learning.

Our second contribution is a novel method for switching between the visual and tactile modes of an STS sensor. Since STS sensors are capable of operating in both visual and tactile modes, the operating mode of the sensor must be switched when contact occurs; this is typically accomplished with a separate algorithm [8]. In this work, we circumvent this requirement by including mode switching as a policy output, allowing the demonstrator to set the sensor mode during the demonstration. In addition to reducing the algorithmic burden of using an STS sensor, we find that this approach effectively learns to switch the sensor at the point of contact, and implicitly verify its effectiveness by observing increased policy performance compared with single-mode sensing.

Finally, we complete an extensive experimental study to evaluate the benefits of including STS proximity and tactile data as inputs to a multimodal control policy. We compare the use of an STS sensor (both with and without mode switching) to the use of an eye-in-hand camera in four different tasks: specifically, the opening and careful closing of two cabinet doors, each with a unique handle or knob.

Our contributions can be summarized as:

- 1) A novel force matching algorithm for improving kinesthetic teaching demonstration data using a Cartesian impedance controller and finger force-torque sensing.
- 2) A novel approach to visual/tactile mode switching when using an STS sensor based on expert demonstrations and a learned policy.
- 3) An extensive experimental study of the benefits of a multimodal visual/tactile sensor for learning policies using IL on a real robotic manipulation platform.

## II. RELATED WORK

Impedance control is an approach to robotic control in which force and position are related as a theoretical mass-spring-damper system [9], and can be seen as a way of achieving a balance between position control and force control, without requiring *a priori* knowledge of environment and contact dynamics. This characteristic makes it a popular choice for many modern robotics applications, but applying desired forces in this scheme can be challenging and typically requires the use of hybrid position/force control instead [10]. We use kinesthetic teaching to generate initial position-only trajectories, and then measured forces with impedance control to generate new trajectories that reproduce both the original path and the applied forces.

Imitation learning is an approach for training a control policy with a set of expert demonstrations. A popular form of

imitation learning is behaviour cloning [11], in which supervised learning is carried out on the expert demonstration set. Behaviour cloning has been used successfully for many tasks in robotic manipulation [6], [12], [13], but recent applications tend to avoid the use of kinesthetic teaching [7], despite its ability to provide direct haptic feedback to the demonstrator. Previous work that combines kinesthetic teaching with force profile reproduction requires one demonstration for positions, and a separate demonstration for forces [14], which can be inconvenient and challenging to provide. In this work, the demonstrator provides a single demonstration including both desired poses and forces through kinesthetic teaching, which is then combined with our novel force matching algorithm to generate our expert dataset.

Gel-based optical tactile sensors have allowed for a wide range of research on dense tactile feedback [2]–[4], [15]. A semi-transparent polymer on top of these sensors has allowed for both visual and tactile sensing [16], and is further improved through the addition of controllable lighting [15]. While these optical sensors can detect many forms of tactile information, a particularly fruitful application is the goal of measuring normal and shear forces through the tracking of printed dots [4], [17], [18] and finite element analysis [4], [17]. In our work, we do not require true metric force, so the complication of the above methods, which require a force-torque sensor for calibration, is unnecessary. We instead estimate a signal proportional to force using an algorithm from concurrently submitted work which provides the surface depth of a tactile sensor based on dot displacement [19].

Learning-based manipulation tasks have benefited from the use of contact sensing [20], as well as optical tactile sensors for both reinforcement learning [21] and imitation learning [22], [23]. Our approach to learning is quite similar to [23], in which tactile, visual, and auditory data is combined in a single neural network and trained with behaviour cloning. In [23], demonstrations are collected primarily with scripts for very specific tasks with a bespoke system. In contrast, we use kinesthetic teaching without any task-based assumptions or scripted policies, which can generalize to many tasks.

Our work is closely related to [8], which uses a multimodal tactile sensor to complete a bead-maze task with a robotic manipulator. In contrast, our tasks require a combination of normal force, shear force, grip, slip, and roll for which it would be difficult to handcraft a policy, so we learn closed-loop motion actions end-to-end with imitation learning instead. Additionally, our policy learns mode switching actions directly, whereas [8] uses a separate model and algorithm

with specific domain knowledge.

### III. METHODOLOGY

In this section, we introduce each component of our system. We will start by providing a brief formulation of imitation learning in the context of a Markov decision process (MDP). Next, we describe our base Cartesian impedance control law and its relationship to kinesthetic teaching. We then present our method to: (i) match expert demonstrator forces, (ii) measure these forces, and (iii) provide sensor mode labels. Finally, we provide our training objective.

#### A. Problem Formulation

A Markov decision process (MDP) is defined as  $\mathcal{M} = \langle \mathcal{S}, \mathcal{A}, R, \mathcal{P}, \rho_0 \rangle$ , where the sets  $\mathcal{S}$  and  $\mathcal{A}$  are respectively the state and action space,  $R : \mathcal{S} \times \mathcal{A} \rightarrow \mathbb{R}$  is a reward function,  $\mathcal{P}$  is the state-transition environment dynamics distribution and  $\rho_0$  is the initial state distribution. Actions are sampled from a stochastic policy  $\pi(a|s)$ . The policy  $\pi$  interacts with the environment to yield experience  $(s_t, a_t, r_t, s_{t+1})$  for  $t = 0, \dots, T$ , where  $s_0 \sim \rho_0(\cdot)$ ,  $a_t \sim \pi(\cdot|s_t)$ ,  $s_{t+1} \sim \mathcal{P}(\cdot|s_t, a_t)$ ,  $r_t = R(s_t, a_t)$ , and  $T$  is the finite horizon length.

We aim to learn a policy  $\pi$  that maximizes the expected return  $J(\pi) = \mathbb{E}_\pi [G(\tau_{0:T})] = \mathbb{E}_\pi \left[ \sum_{t=0}^T \gamma^t R(s_t, a_t) \right]$ , where  $\tau_{t:T} = \{(s_t, a_t), \dots, (s_T, a_T)\}$  is the trajectory starting with  $(s_t, a_t)$ , and  $G(\tau_{t:T})$  is the return of trajectory  $\tau$ .

In this work, we focus on imitation learning (IL), where  $R$  is unknown and instead we are given a finite set of task-specific expert demonstration  $(s, a)$  pairs  $\mathcal{B}_E = \{(s, a), \dots\}$ .

#### B. Data Collection with Kinesthetic Teaching

We collect  $\mathcal{B}_E$  for each task separately using kinesthetic teaching, in which the expert physically pushes the robot to collect demonstrations. A popular means of implementing kinesthetic teaching is with a torque-controlled robot running a cartesian impedance controller. The cartesian impedance controller motion equation is

$$\mathcal{F} = \mathbf{K}\mathbf{e}^x + \mathbf{D}\dot{\mathbf{e}}^x + \mathbf{\Lambda}\ddot{\mathbf{e}}^x + \boldsymbol{\mu}(\mathbf{q}, \dot{\mathbf{q}}), \quad (1)$$

where  $\mathcal{F}$  represents the generalized force,  $\mathbf{e}^x = \mathbf{x}^d - \mathbf{x}$  is the difference between desired and current pose<sup>1</sup>,  $\mathbf{K}$  and  $\mathbf{D}$  are the manually tuned stiffness and damping diagonal matrices,  $\mathbf{\Lambda}$  is the fixed inertia matrix, determined based on known end-effector parameters, and  $\boldsymbol{\mu}(\mathbf{q}, \dot{\mathbf{q}})$  is a term encompassing generalized force of Coriolis, centrifugal, and gravitation based on current joint positions and velocities,  $\mathbf{q}$  and  $\dot{\mathbf{q}}$ . In our case,  $\mathcal{F}$  is a six-dimensional wrench since we control the robot in six degrees of freedom (three translational, three rotational). To allow kinesthetic teaching demonstrations, we set  $\mathbf{K}$  and  $\mathbf{D}$  very close to zero, ensuring the robot has full compliance with the environment, while  $\mathbf{\Lambda}(\ddot{\mathbf{e}}^x)$  and  $\boldsymbol{\mu}(\mathbf{q}, \dot{\mathbf{q}})$  handle gravity compensation.

A standard approach to kinesthetic teaching involves recording the end-effector poses  $\mathbf{x}_E$  at a fixed rate as the

<sup>1</sup>We handle rotational pose components with conversions between rotation vectors and quaternions, but leave this out of our methodology for brevity.

robot is moved by the expert, and using these poses (or changes between poses) as expert actions [5]. Indeed, this is one part of our approach, but it suffers from at least two limitations: (i) recording these positions as the robot is moved means that the corresponding states and actions may not accurately reflect  $\mathcal{S}$  and  $\mathcal{A}$ , and (ii) if the expert generates motion in which a wrench is applied between the robot and the environment with no corresponding change in  $\mathbf{x}_E$ , this approach will fail to reproduce that wrench.

The first issue above can be resolved with *replays*, in which the demonstrator collects a single demonstration trajectory  $\tau_{x,E-\text{raw}} = \{\mathbf{x}_{E-\text{raw},0}, \dots, \mathbf{x}_{E-\text{raw},T}\}$ , resets the environment to the same  $s_0$ , and then uses a sufficiently accurate controller to reproduce each  $\mathbf{x}_{E-\text{raw}}$  [24]. Resolving the second issue requires additional sensory input, which we describe in the following section.

#### C. Force Matching

If the contact wrench at the end-effector can be accurately measured, then we can modify the demonstrated trajectories based on this wrench to ensure that the expert demonstrator's force and torque are matched in a replayed trajectory. Consider a raw demonstrator trajectory of recorded end-effector poses  $\tau_{x,E-\text{raw}}$  and wrenches  $\tau_{f,E-\text{raw}} = \{\mathcal{F}_{E-\text{raw},0}, \dots, \mathcal{F}_{E-\text{raw},T}\}$  as a set of poses and wrenches that we would like our controller to achieve. We will further consider the case where each desired pose is in static equilibrium, where Eq. (1) simplifies to

$$\mathcal{F}_{E-\text{raw},t} = \mathbf{K}\mathbf{e}_{E-\text{raw},t}^x, \quad (2)$$

rearranged to set new desired replay poses as

$$\mathbf{x}_{E-\text{rep},t}^d = \mathbf{K}^{-1} \mathcal{F}_{E-\text{raw},t} + \mathbf{x}_{E-\text{raw},t}, \quad (3)$$

where we have used  $\mathbf{e}_{E-\text{raw},t}^x = \mathbf{x}_{E-\text{rep},t}^d - \mathbf{x}_{E-\text{raw},t}$ .

We consider the stiffness  $\mathbf{K}$  to be a fixed hyperparameter (typically a diagonal matrix with one value for all translational components, and another for all rotational ones), selected to optimally trade off control accuracy and environment compliance. Using Eq. (3), we can generate a desired replay trajectory  $\tau_{x,E-\text{rep}}^d = \{\mathbf{x}_{E-\text{rep},0}^d, \dots, \mathbf{x}_{E-\text{rep},T}^d\}$ , a new set of poses that, under static conditions, would reproduce the forces from  $\tau_{f,E-\text{raw}}$ . In reality, we desire smooth, continuous motion and this simplification does not account for dynamic effects. Experimentally, we find that when we input  $\tau_{x,E-\text{rep}}^d$  as a set of desired poses for our Cartesian impedance controller, we achieve *replayed* trajectories  $\tau_{x,E-\text{rep}}$  and  $\tau_{f,E-\text{rep}}$  that sufficiently match  $\tau_{x,E-\text{raw}}$  and  $\tau_{f,E-\text{raw}}$ .

#### D. Force Measurement

To generate  $\tau_{x,E-\text{rep}}^d$  with Eq. (3), we require a means of sensing environment-robot forces  $\tau_{f,E-\text{raw}}$ . Common approaches for sensing end-effector forces on robotic arms include the use of wrist-mounted force-torque sensors or joint-torque sensors with dynamics modelling. In both of these cases,  $\tau_{f,E-\text{raw}}$  provides a signal corrupted by the demonstrator's own force against the robot (see Fig. 3). To avoid this corruption, a sensor must be mounted at a

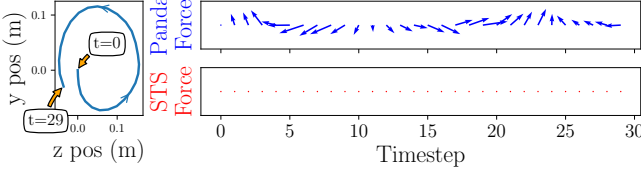


Fig. 3: Example expert demonstrations showing measured forces with Panda (the robot) joint-torque sensors and dynamics modelling (blue) and our own sensor (red) (collapsed from full 6-DOF to 2-DOF for viewing purposes). The left and right trajectories correspond to the arm being (i) pushed in a circle (without environmental contact) and (ii) towards, against, and away from a fixed knob, respectively. The STS sensor correctly shows no readings in (i), where there is no contact, and shows increasing and then decreasing force during contact in (ii). See supplementary materials for corresponding video.

point on the end-effector where human-applied forces are ignored during demonstrations, such as on the finger of a gripper. While finger-mounted force-torque sensors exist, we use an optical tactile sensor because: (i) they are more widely available due to their order-of-magnitude lower cost (one thousand to five thousand dollars vs. approximately one hundred dollars), (ii) the rich signal from the tactile sensor can separately be used for learning control policies, and (iii) we do not require true, metric force  $\mathcal{F}$ , but rather a signal that is simply *proportional* to force,  $\tilde{\mathcal{F}}$ .

Addressing the third point, we calibrate our sensor using a scripted policy to incrementally push the sensor against the static environment numerous times, providing small initial perturbations to each trajectory to increase robustness. Throughout these trajectories, we measure and record  $\tilde{\mathcal{F}}$  and  $e^x$ —the measured calibration values and the piecewise linear relationship between the two for normal forces  $\tilde{\mathcal{F}}^{(z\text{-ax})}$  is shown in Fig. 4. We elect to use a piecewise linear model, as the relationship between surface depth and normal force for optical tactile sensors has previously been shown to be linear [17], though a more accurate model may exist. The simplified relationship is

$$\tilde{\mathcal{F}} = \mathbf{A}_{\tilde{\mathcal{F}}e} e + \mathbf{b}_{\tilde{\mathcal{F}}e}, \quad (4)$$

which can be rearranged as a modified version of Eq. (3) to

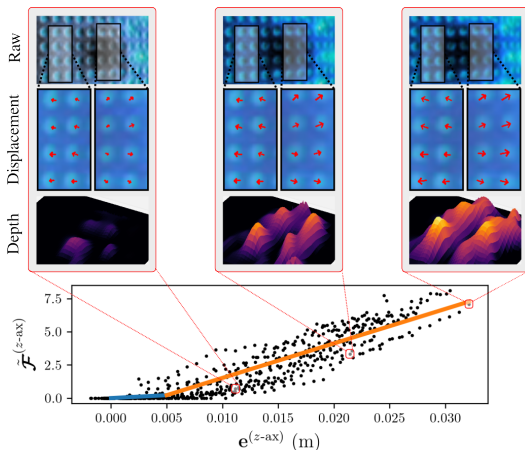
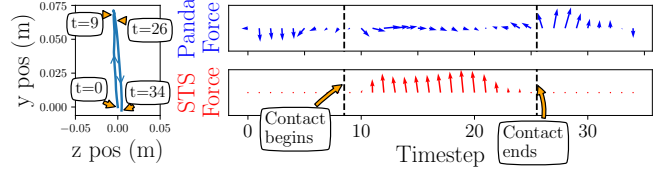


Fig. 4: Example raw images, marker displacement, and inferred depth [19] for three recorded  $e^{(z\text{-ax})}$  and  $\tilde{\mathcal{F}}^{(z\text{-ax})}$  values, along with the piecewise linear relationship between  $e^{(z\text{-ax})}$  and  $\tilde{\mathcal{F}}^{(z\text{-ax})}$ . See supplementary materials for corresponding video.



yield  $\tau_{x,E\text{-rep}}^d$ :

$$\mathbf{x}_{E\text{-rep},t}^d = \mathbf{A}_{\tilde{\mathcal{F}}e}^{-1} (\tilde{\mathcal{F}}_{E\text{-raw},t} - \mathbf{b}_{\tilde{\mathcal{F}}e}) + \mathbf{x}_{E\text{-raw},t}. \quad (5)$$

During kinesthetic teaching, we keep our sensor in tactile mode for reading  $\tilde{\mathcal{F}}$ , and only allow mode switching during replays, when reading  $\tilde{\mathcal{F}}$  is no longer required.

We measure these signals proportional to forces in a variety of ways, depending on the specific degree of freedom. For normal force, we use a method for estimating membrane depth, where depth is inferred from marker movement on the surface of the membrane, as shown in Fig. 4 [19]. Using a perspective camera model, [19] models a relationship between the separation of markers locally, and the amount of displacement towards the camera, allowing dense 2.5D depth to be recovered using properties of a local distance transform. We use average depth for  $\tilde{\mathcal{F}}$ . Fig. 4 shows examples of both dot displacement and corresponding estimated depth at all points as the knob is pushed against the sensor. For signals proportional to shear forces and torque about the normal axis, we use the average of the tracked dot movement, while simultaneously estimating a centre point for torque. We do not measure torque about the axes parallel to the surface, but experimentally find these extra degrees of freedom are not necessary for generating a successful  $\tau_{x,E\text{-rep}}$ .

#### E. STS Sensor Mode Labelling

After each kinesthetic teaching trajectory, the expert adds STS sensor mode labels during the replay phase. As the controller autonomously generates  $\tau_{x,E\text{-rep}}$ , the demonstrator observes and presses a button to change the sensor mode, typically as close to the point of contact as possible. These labels are recorded and used to train policy outputs.

#### F. Policy Training

Our policies are trained with a standard mean-squared-error behaviour cloning loss,

$$\mathcal{L}(\pi) = \sum_{(s,a) \in \mathcal{B}^E} (\pi(s) - a)^2, \quad (6)$$

where  $s \in \mathcal{S}$  and  $a \in \mathcal{A}$ . See Section IV-A for more details about  $\mathcal{S}$  and  $\mathcal{A}$ .

## IV. EXPERIMENTS

We complete a variety of experiments to verify the efficacy of our force matching algorithm and our mode-switching policy output. We also perform experiments with many

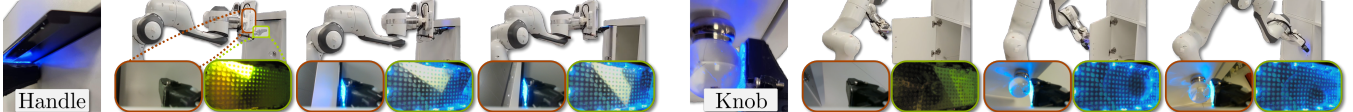


Fig. 5: Example partial trajectories and sensor data for our Flat Handle and Glass Knob Close tasks. All tasks have an initial reaching component before the door is opened or closed. See supplementary video for full examples.

different observation configurations to evaluate the value of including STS data in a learned policy.

#### A. Environment and Task Parameters

We choose to examine cabinet door opening and closing, using one door with a flat handle and one with a spherical knob, giving us four total experimental tasks. All tasks include an initial reaching component (see Fig. 5). Door opening tasks are considered successful if the door fully opens within a given time limit. Door closing tasks are considered successful if the door closes without “slamming” because the knob or handle slips from the finger, which occurs because the doors are mounted with spring hinges.

Our robotic platform is a Franka Emika Panda, and we use the default controller that comes with Polymetis [25] as our Cartesian impedance controller. For all tasks, at the beginning of each episode, the initial pose of the end-effector frame is randomized to be within a  $3\text{ cm} \times 3\text{ cm} \times 3\text{ cm}$  cube in free space, with the rotation about the global  $z$ -axis randomized between  $-0.15$  and  $+0.15$  radians. Our task environments can include wrist camera  $212 \times 120$  pixel RGB images, raw  $212 \times 120$  STS images, and the current and previous relative end-effector poses (position, quaternion). In this case, *relative* means that in each episode, the initial pose is set to  $\{0, 0, 0, 0, 0, 0, 1\}$ . These choices were meant to simulate the scenario in which an approximate reach is performed with an existing policy and global pose information between episodes is inconsistent (e.g., in the case of a mobile manipulator in a larger environment).

Our sensor is based on the one developed in [8], but in a smaller form factor. The finger housing is 3D printed and mounted on the Franka Emika Panda gripper.

Demonstrations are collected by allowing a user to press a button, switching the stiffness and damping on the controller to nearly zero, and then data is collected at a predefined rate (10 Hz in our experiments) once a minimum motion threshold (0.5 mm in our experiments) is met. After the kinesthetic demonstration is completed, the environment is reset to the same initial pose, and the demonstration is replayed, optionally using altered desired poses to allow force matching (see Sections III-C and III-D), also allowing the user to provide a mode-switch label (see Section III-E).

#### B. Policy Performance

We collected data and trained policies in a variety of configurations to evaluate our force matching and mode switching contributions, as well as the benefits of including multimodal tactile data for policy learning. The configuration labels are:

- **FM:** force matching.

- **MS, TO, VO:** mode switching, tactile-only, visual-only.
- **WSR:** wrist camera, STS, relative pose in observation. Excluded letters are excluded from the observation (e.g. WR: wrist camera, relative pose, no STS).

For our experiments, each dataset only requires a single set of human demonstrations, and we can then replay those demonstrations for different configurations. The different configurations are whether or not FM is used, and whether the sensor is set to MS, TO, or VO; training with a different observation space does not require the collection of a new dataset. The ability to replay a single set of human demonstrations means that our experiments require a relatively small amount of human data (about two minutes per task), and also ensures that each environment configuration is compared on equivalent human trajectories. Each dataset contains 20 (replayed) trajectories, and for each configuration (see Fig. 6 and Fig. 8 for tested configurations), we trained and tested three random seeds for 10 episodes per seed.

We trained our policies in PyTorch with the Adam optimizer and a learning rate of 0.0003, halving the learning rate halfway through training. We use a ResNet-18 architecture pretrained on ImageNet and ending with spatial soft-argmax [26] for image data, and a small fully connected network for relative pose data. Features from each modality are concatenated and passed through another small fully connected network before outputting our seven-dimensional action: relative position change, orientation change as a rotation vector, and STS mode. All layers use ReLU nonlinearities. We train each policy for 20k gradient steps, using weight decay of 0.1 to avoid overfitting, as this has been shown to significantly improve behaviour cloning results in

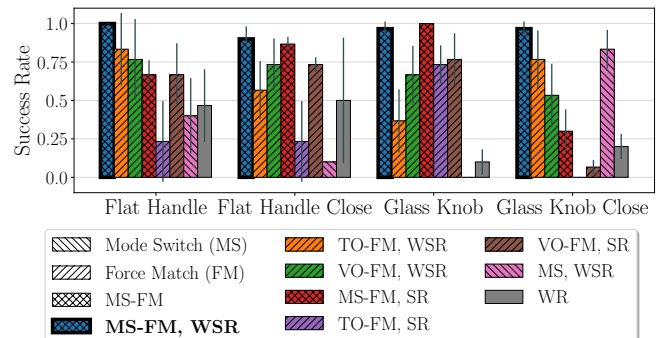


Fig. 6: Performance results with different configurations for evaluating force matching and STS mode switching, illustrating the overall benefit of adding both mode switching and force matching. MS: mode switching, TO: tactile-only, VO: visual-only, and FM: force matching. For the observation space, W: wrist camera, S: STS, and R: relative pose. The black lines show standard deviation of seeds. The configuration with both novel additions (MS and FM) and all sensing modalities (WSR) is shown in bold.

recent work compared to early stopping [12], [27].

1) *Force Matching and Mode Switching*: The results of testing force matching and mode switching on learned policies are shown in Fig. 6. To evaluate force matching, we compare MS-FM, WSR policies against policies learned without force matching but with mode switching (MS, WSR), as well as a baseline that does not use force matching, mode switching, or STS visual/tactile data (WR). The mean success rates and standard deviations across all tasks for these three variants (120 episodes/variant total) are 0.96 (0.064), 0.33 (0.35), and 0.32 (0.30), respectively, illustrating that force matching provides a clear performance boost.

To evaluate mode switching, we compare against policies that exclusively use a single mode: tactile-only (TO) or visual-only (VO). Using only a single mode deteriorates policy performance in all cases. With wrist observations included (WSR), the difference in performance between visual-only and tactile-only can most likely be explained by whether the wrist camera can provide enough information to consistently complete the initial reach. When excluding wrist observations (SR), VO policies outperform TO policies, likely because the initial reach may not be possible when the sensor is in tactile mode (see Fig. 7).

2) *Observation Space Study*: The results of our observation space ablation study are shown in Fig. 8. For these tests, we do not have to create any new datasets, and only train new policies using the same data from Section IV-B.1. Given the clear benefits of force matching, all policies in this figure used force matching, and mode switching if they include an STS sensor. We include relative pose alone as a baseline to show that, due to the initial randomization described in Section IV-A, the tasks require visual feedback to succeed consistently, and that a single “average” trajectory combined with impedance control is not, by itself, effective.

The clearest conclusion from these results is that a combination of wrist camera, STS, and relative pose data performs most consistently well. Particularly in the Glass Knob Close task, the loss of any of these modalities causes a significant drop in performance. This is further supported by the perhaps surprisingly high performance of the “Wrist, STS” policy (which excludes relative pose data), since relative pose provides a strong prior for what section of the task is currently being completed. Other performance differences

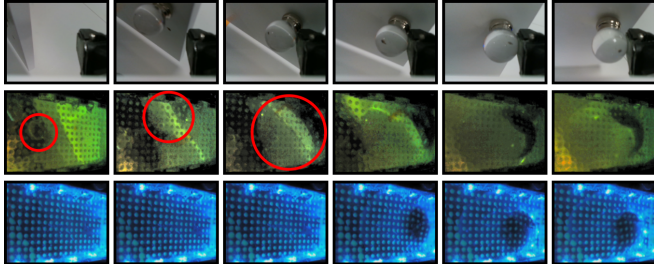


Fig. 7: A single Glass Knob Close trajectory with STS data in visual-only (knob highlighted with red circle) and tactile-only modes, illustrating the necessity of both. The corresponding wrist camera data is provided at the top for reference. See supplementary materials for corresponding video.

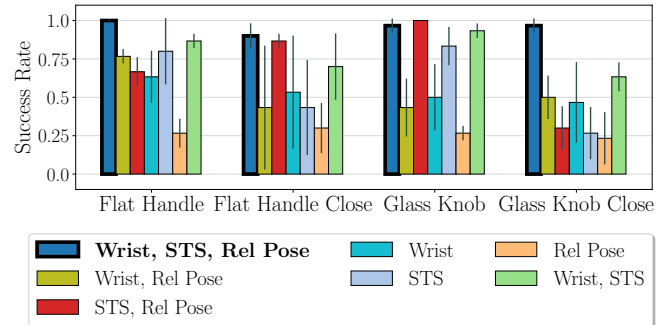


Fig. 8: Performance for different observation spaces to evaluate the utility of tactile (STS) data. All variants in this figure use force matching and, if they include an STS sensor, mode switching. The black lines show standard deviation of seeds. The configuration with all sensing modalities is shown in bold.

between sensing modalities can, again, be partially explained by the particular challenges presented by each individual task: for example, the Glass Knob (open) task performs quite well with just STS data and poorly with wrist camera data. A possible explanation is that the knob must be pushed with a high amount of force to pull the door open in this task, and the wrist camera alone does not accurately provide this feedback.

3) *Expert Data Scaling*: Fig. 9 shows the results of experiments with lower amounts of training data in a subset of the conditions from Section IV-B.1 and Section IV-B.2. Most methods improve with increased data, but there are exceptions. For example, both STS-free methods do not improve significantly with increasing data for Flat Handle Close, Glass Knob, or Glass Knob Close, which indicates that eye-in-finger visual data, as well as tactile data, are beneficial to these tasks. A surprising finding is that for Flat Handle, Flat Handle Close, and Glass Knob, performance is quite good for MS-FM, WSR even with only five demonstrations, though there is a gradual increase in performance with more data. Performance on our hardest task, Glass Knob Close, clearly increases with more data.

### C. Force Matching

While our policy learning experiments in Section IV-B implicitly illustrate the value of force matching through improved performance, Fig. 10 shows specific examples:

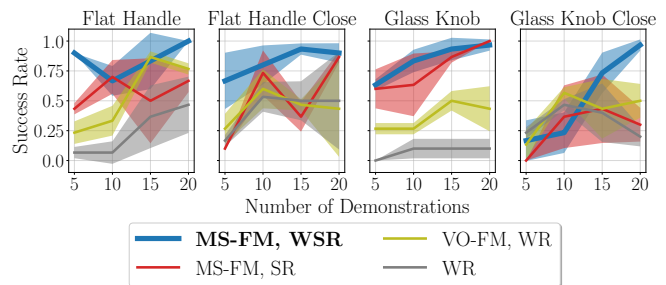


Fig. 9: Performance with varying amounts of expert data for a subset of the conditions in Fig. 6 and Fig. 8. The shading shows standard deviation of seeds. The configuration with both novel additions (MS and FM) and all sensing modalities (WSR) is shown in bold.

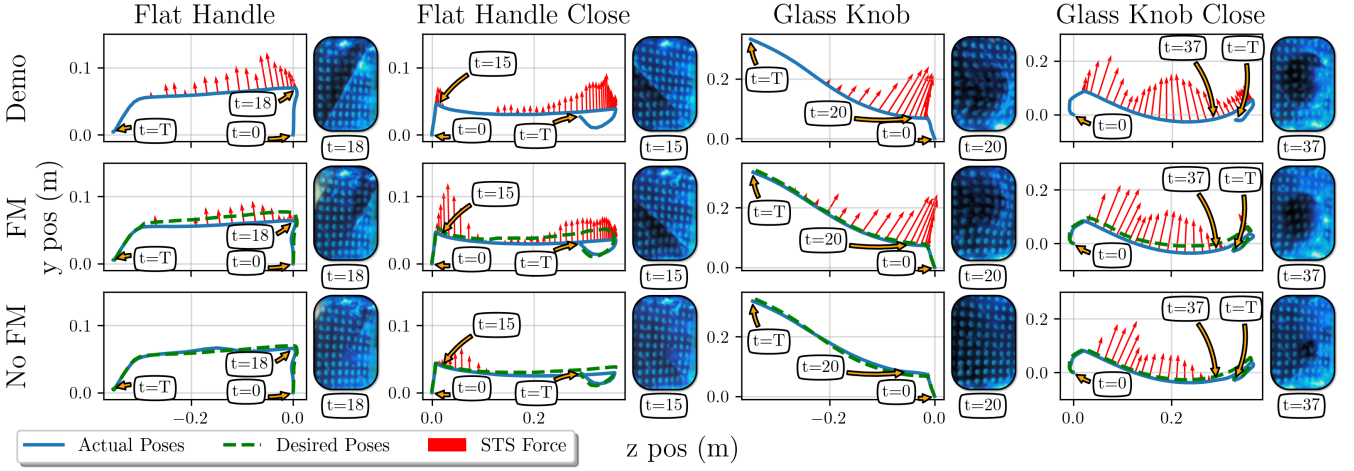


Fig. 10: Example demonstrator trajectories with and without force matching (FM). Notice how, in the FM row, the difference between the desired pose and the actual pose generates increased STS force compared with the No FM row (as described by Eq. (5)). Our algorithm qualitatively (example images) and quantitatively (measured STS force) better matches the original demonstrator trajectory. See supplementary materials for corresponding video.

- Top: a raw demonstration trajectory  $\tau_{x,E\text{-raw}}$  (blue) as well as demonstration forces  $\tau_{\tilde{f},E\text{-raw}}$  (red).
- Middle: a new set of desired poses that incorporate force matching  $\tau_{x,E\text{-rep}}^d$  (green), the new set of replayed poses  $\tau_{x,E\text{-rep}}$  given  $\tau_{x,E\text{-rep}}^d$  (blue), and the actual forces with the modified trajectory  $\tau_{\tilde{f},E\text{-rep}}$  (red).
- Bottom: a set of desired and actual poses, along with resulting forces, that use  $\tau_{x,E\text{-raw}}$  directly, while ignoring  $\tau_{\tilde{f},E\text{-raw}}$ , to generate a replay (green, blue, and red, respectively).

We label the initial timestep  $t = 0$ , final timestep  $t = T$ , and a single representative timestep for each trajectory, also including a cropped STS image at the representative timestep for each trajectory. Notice that the No FM desired poses (bottom, green) are exactly the same as the true demo poses (top, blue). In each of these four cases, the No FM replay caused the end-effector to slip off of the handle or knob, causing the task to not be completed successfully.

Overall, it is clear that force matching generates  $\tau_{x,E\text{-rep}}$  and  $\tau_{\tilde{f},E\text{-rep}}$  that better match  $\tau_{x,E\text{-raw}}$  and  $\tau_{\tilde{f},E\text{-raw}}$ . While  $\tau_{\tilde{f},E\text{-rep}}$  occasionally has mismatches with  $\tau_{\tilde{f},E\text{-raw}}$ , much of these errors can be attributed to a combination of sensor reading errors (see right side of Fig. 4) and control errors. With

improved sensing and control accuracy, these mismatches would be significantly reduced, although a model that incorporates dynamic effects would be required to perfectly reproduce  $\tau_{x,E\text{-raw}}$  and  $\tau_{\tilde{f},E\text{-raw}}$ .

#### D. Mode Switching

In addition to the results from our policy learning experiments (Section IV-B), we completed a short analysis to evaluate our learned mode switch action. As context, we will consider that an optimal switch occurs at the moment of contact.

For each MS-FM, WSR dataset, we recorded the timestep at which contact was made between the handle/knob and the surface of the STS, and compared that to the timestep that the demonstrator provided a mode switch action label. The histograms of these timestep differences are shown in the top row of Fig. 11. While there are arguably certain task-specific patterns, such as a slightly higher timestep difference average for the handle tasks, the clearest pattern is that the mode switch label typically occurs within one timestep (0.1 s) of contact being made. The bottom row shows the same analysis, but for autonomous policies. With the exception of a few outliers (particularly in Flat Handle), the policies have converged to be closer to an average of zero timesteps between contact and mode switching, smoothing out the reaction time errors from the expert dataset. The outliers in Flat Handle are mostly caused by a causal mismatch, where occasionally the policy learns to switch modes based on when the arm starts opening the handle, instead of at the moment of contact.

## V. LIMITATIONS

Our method and experiments are not without limitations. Although we used a single sensor for all of our experiments, the gel-based contact surface of the STS physically degrades over time. This limitation partially motivates the use of learned models for gel-based sensors; if sensor data changes marginally due to degradation, a practitioner can merely add

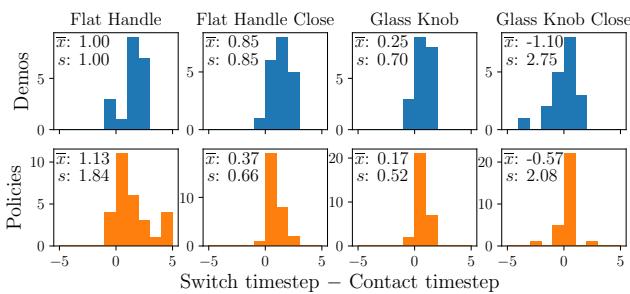


Fig. 11: Histograms of the difference between mode switch action timestep and the true first contact timestep, for both our demonstrations and our learned MS-FM, WSR policies.

more data to the dataset and retrain the policy. As well, the STS uses a standard visual camera, so policies trained on its data are susceptible to the same problems as other visual data paired with neural networks, such as overfitting to specific lighting conditions. Finally, our force-matched replayed demonstrations still occasionally fail because both our method for measuring forces as well as our Cartesian impedance controller can suffer from accuracy issues, but both of these limitations can be improved with further tuning.

## VI. CONCLUSION

We presented an imitation learning system that combines kinesthetic teaching with Cartesian impedance control through the use of force matching, leveraging an optical tactile sensor to read a signal proportional to force. On real-world manipulation tasks, we showed the benefits of using a multimodal sensor in particular, where reaching can be accomplished in a visual mode, while a tactile mode handles contact. We demonstrated the efficacy of learning an action for switching between visual and tactile modes end-to-end as an addition to a motion action. We used this system to learn policies for four challenging cabinet opening and closing tasks, and completed an exhaustive study of different configurations and observation spaces to verify the effectiveness of force matching, sensor mode switching, and tactile sensing in general. Potential directions for future work include improving the accuracy of our force sensing method or adding a means for self-improvement by detecting execution failures.

## REFERENCES

- [1] C. Chi, X. Sun, N. Xue, T. Li, and C. Liu, “Recent Progress in Technologies for Tactile Sensors,” *Sensors*, vol. 18, no. 4, p. 948, Apr. 2018.
- [2] W. Yuan, S. Dong, and E. H. Adelson, “GelSight: High-Resolution Robot Tactile Sensors for Estimating Geometry and Force,” *Sensors*, vol. 17, no. 12, p. 2762, Dec. 2017.
- [3] A. Padmanabha, F. Ebert, S. Tian, R. Calandra, C. Finn, and S. Levine, “OmniTact: A Multi-Directional High-Resolution Touch Sensor,” in *2020 IEEE International Conference on Robotics and Automation (ICRA)*, May 2020, pp. 618–624.
- [4] D. Ma, E. Donlon, S. Dong, and A. Rodriguez, “Dense Tactile Force Estimation using GelSlim and inverse FEM,” in *2019 International Conference on Robotics and Automation (ICRA)*, May 2019, pp. 5418–5424.
- [5] A. G. Billard, S. Calinon, and R. Dillmann, “Learning from Humans,” in *Springer Handbook of Robotics*, B. Siciliano and O. Khatib, Eds. Cham: Springer International Publishing, 2016, pp. 1995–2014.
- [6] T. Ablett, Y. Zhai, and J. Kelly, “Seeing All the Angles: Learning Multiview Manipulation Policies for Contact-Rich Tasks from Demonstrations,” in *Proceedings of the IEEE/RSJ International Conference on Intelligent Robots and Systems (IROS’21)*, Prague, Czech Republic, Sept. 2021.
- [7] K. Li, D. Chappell, and N. Rojas, “Immersive Demonstrations are the Key to Imitation Learning,” Jan. 2023.
- [8] F. R. Hogan, J.-F. Tremblay, B. H. Baghi, M. Jenkin, K. Siddiqi, and G. Dudek, “Finger-STS: Combined Proximity and Tactile Sensing for Robotic Manipulation,” *IEEE Robotics and Automation Letters*, vol. 7, no. 4, pp. 10 865–10 872, Oct. 2022.
- [9] N. Hogan, “Impedance Control: An Approach to Manipulation,” in *1984 American Control Conference*, June 1984, pp. 304–313.
- [10] M. H. Raibert and J. J. Craig, “Hybrid Position/Force Control of Manipulators,” *Journal of Dynamic Systems, Measurement, and Control*, vol. 103, no. 2, pp. 126–133, June 1981.
- [11] M. Bain and C. Sammut, “A Framework for Behavioural Cloning,” in *Machine Intelligence 15*. Oxford University Press, 1996, pp. 103–129.
- [12] A. Mandlekar, *et al.*, “What Matters in Learning from Offline Human Demonstrations for Robot Manipulation,” in *Conference on Robot Learning*, Nov. 2021.
- [13] T. Zhang, *et al.*, “Deep Imitation Learning for Complex Manipulation Tasks from Virtual Reality Teleoperation,” in *Proceedings of the IEEE International Conference on Robotics and Automation (ICRA’18)*. Brisbane, QLD, Australia: IEEE, May 2018, pp. 5628–5635.
- [14] P. Kormushev, S. Calinon, and D. G. Caldwell, “Imitation Learning of Positional and Force Skills Demonstrated via Kinesthetic Teaching and Haptic Input,” *Advanced Robotics*, vol. 25, no. 5, pp. 581–603, Jan. 2011.
- [15] F. R. Hogan, M. Jenkin, S. Rezaei-Shoshtari, Y. Girdhar, D. Meger, and G. Dudek, “Seeing Through your Skin: Recognizing Objects with a Novel Visuotactile Sensor,” Dec. 2020.
- [16] A. Yamaguchi and C. G. Atkeson, “Implementing tactile behaviors using FingerVision,” in *2017 IEEE-RAS 17th International Conference on Humanoid Robotics (Humanoids)*, Nov. 2017, pp. 241–248.
- [17] W. Yuan, “Tactile Measurement with a GelSight Sensor,” Master’s thesis, Massachusetts Institute of Technology, 2014.
- [18] W. Kim, W. D. Kim, J.-J. Kim, C.-H. Kim, and J. Kim, “UVtac: Switchable UV Marker-Based Tactile Sensing Finger for Effective Force Estimation and Object Localization,” *IEEE Robotics and Automation Letters*, vol. 7, no. 3, pp. 6036–6043, July 2022.
- [19] A. Jilani, “Direct Shape from Touch Sensing,” Master’s Thesis [in Progress], McGill University, Sept. 2023.
- [20] Y. Chebotar, O. Kroemer, and J. Peters, “Learning robot tactile sensing for object manipulation,” in *2014 IEEE/RSJ International Conference on Intelligent Robots and Systems*, Sept. 2014, pp. 3368–3375.
- [21] J. Hansen, F. Hogan, D. Rivkin, D. Meger, M. Jenkin, and G. Dudek, “Visuotactile-RL: Learning Multimodal Manipulation Policies with Deep Reinforcement Learning,” in *2022 International Conference on Robotics and Automation (ICRA)*, May 2022, pp. 8298–8304.
- [22] I. Huang and R. Bajcsy, “Robot Learning from Demonstration with Tactile Signals for Geometry-Dependent Tasks,” in *2020 IEEE/RSJ International Conference on Intelligent Robots and Systems (IROS)*. Las Vegas, NV, USA: IEEE, Oct. 2020, pp. 8323–8328.
- [23] H. Li, *et al.*, “See, Hear, and Feel: Smart Sensory Fusion for Robotic Manipulation,” in *6th Annual Conference on Robot Learning*, Nov. 2022.
- [24] S. Dasari, *et al.*, “RB2: Robotic Manipulation Benchmarking with a Twist,” in *Thirty-Fifth Conference on Neural Information Processing Systems Datasets and Benchmarks Track (Round 2)*, Oct. 2021.
- [25] Y. Lin, A. S. Wang, G. Sutanto, A. Rai, and F. Meier, “Polymetis,” <https://facebookresearch.github.io/fairo/polymetis/>, 2021.
- [26] S. Levine, C. Finn, T. Darrell, and P. Abbeel, “End-to-end training of deep visuomotor policies,” *Journal of Machine Learning Research*, vol. 17, no. 39, pp. 1–40, 2016.
- [27] T. Ablett, B. Chan, and J. Kelly, “Learning From Guided Play: Improving Exploration for Adversarial Imitation Learning With Simple Auxiliary Tasks,” *IEEE Robotics and Automation Letters*, vol. 8, no. 3, pp. 1263–1270, Mar. 2023.